



**HAL**  
open science

**A first assessment of the SMOS data in southwestern France using in situ and airborne soil moisture estimates: the CAROLS airborne campaign**

Clément Albergel, Elena Zakharova, Jean-Christophe Calvet, Mehrez Zribi, Mickaël Pardé, Jean-Pierre Wigneron, Nathalie Novello, Yann H. Kerr, Arnaud Mialon, Nouredine Fritz

► **To cite this version:**

Clément Albergel, Elena Zakharova, Jean-Christophe Calvet, Mehrez Zribi, Mickaël Pardé, et al.. A first assessment of the SMOS data in southwestern France using in situ and airborne soil moisture estimates: the CAROLS airborne campaign. *Remote Sensing of Environment*, 2011, 115 (10), pp.2718-2728. 10.1016/j.rse.2011.06.012 . ird-00610348

**HAL Id: ird-00610348**

**<https://ird.hal.science/ird-00610348v1>**

Submitted on 21 Jul 2011

**HAL** is a multi-disciplinary open access archive for the deposit and dissemination of scientific research documents, whether they are published or not. The documents may come from teaching and research institutions in France or abroad, or from public or private research centers.

L'archive ouverte pluridisciplinaire **HAL**, est destinée au dépôt et à la diffusion de documents scientifiques de niveau recherche, publiés ou non, émanant des établissements d'enseignement et de recherche français ou étrangers, des laboratoires publics ou privés.

# 1 A first assessment of the SMOS data in southwestern 2 France using in situ and airborne soil moisture 3 estimates: the CAROLS airborne campaign 4

5 Clément Albergel<sup>(1,2)</sup>, Elena Zakharova<sup>(1)</sup>, Jean-Christophe Calvet<sup>(1)</sup>, Mehrez Zribi<sup>(3-4)</sup>,  
6 Mickaël Pardé<sup>(4)</sup>, Jean-Pierre Wigneron<sup>(5)</sup>, Nathalie Novello<sup>(5)</sup>, Yann Kerr<sup>(3)</sup>, Arnaud  
7 Mialon<sup>(3)</sup>, Nour-ed-Dine Fritz<sup>(1)</sup>

8  
9 [1] CNRM-GAME, Météo-France, CNRS, URA 1357, 42 avenue Gaspard Coriolis,  
10 Toulouse, France,

11 [2] Now at ECMWF, Shinfield Park, Reading UK,

12 [3] CESBIO, CNES/CNRS/IRD/UPS, UMR 5126, 18 Avenue Edouard Belin, Toulouse,  
13 France,

14 [4] LATMOS/CNRS, 10-12 av. de l'Europe, Vélizy, France

15 [5] INRA, EPHYSE, 71 avenue Edouard Bourlaux, Villenave d'Ornon, France,

16

17 Correspondence to: J.-C. Calvet ([jean-christophe.calvet@meteo.fr](mailto:jean-christophe.calvet@meteo.fr))

18

19 **Abstract** - The Soil Moisture and Ocean Salinity (SMOS) satellite mission, based on an  
20 aperture synthesis L-band radiometer was successfully launched in November 2009. In the  
21 context of a validation campaign for the SMOS mission, intensive airborne and in situ  
22 observations were performed in southwestern France for the SMOS CAL/VAL, from April to  
23 May 2009 and from April to July 2010. The CAROLS (Cooperative Airborne Radiometer for  
24 Ocean and Land Studies) bi-angular ( $34^{\circ}$ - $0^{\circ}$ ) and dual-polarized (V and H) L-band radiometer  
25 was designed, built and installed on board the French ATR-42 research aircraft. During  
26 springs of 2009 and 2010, soil moisture observations from the SMOSMANIA (Soil Moisture

27 Observing System – Meteorological Automatic Network Integrated Application) network of  
28 Météo-France were complemented by airborne observations of the CAROLS L-band  
29 radiometer, following an Atlantic-Mediterranean transect in southwestern France.  
30 Additionally to the 12 stations of the SMOSMANIA soil moisture network, in situ  
31 measurements were collected in three specific sites within an area representative of a SMOS  
32 pixel. Microwave radiometer observations, acquired over southwestern France by the  
33 CAROLS instrument were analyzed in order to assess their sensitivity to surface soil moisture  
34 ( $w_g$ ). A combination of microwave brightness temperature ( $T_b$ ) at either two polarizations or  
35 two contrasting incidence angles was used to retrieve  $w_g$  through regressed empirical  
36 logarithmic equations with good results, depending on the chosen configuration. The  
37 regressions derived from the CAROLS measurements were applied to the SMOS  $T_b$  and their  
38 retrieval performance was evaluated. The retrievals of  $w_g$  showed significant correlation ( $p$ -  
39 value  $< 0.05$ ) with surface measurements for most of the SMOSMANIA stations (8 of 12  
40 stations) and with additional field measurements at two specific sites, also. Root mean square  
41 errors varied from 0.03 to 0.09  $\text{m}^3\text{m}^{-3}$  (0.06  $\text{m}^3\text{m}^{-3}$  on average).

42

## 44 **1. Introduction**

45 Soil moisture controls both evaporation and transpiration from bare soil and vegetated areas,  
46 respectively, playing a key role in the interactions between the hydrosphere, the biosphere and  
47 the atmosphere. As a consequence, a significant amount of studies have been and are  
48 currently conducted to obtain soil moisture estimates. For that purpose, land surface modeling  
49 (Dirmeyer et al., 1999, Georgakakos and Carpenter 2006 among others) and remote sensing  
50 techniques (Wagner et al., 1999, 2007; Kerr et al., 2001, 2007; Njoku et al., 2003) are used.  
51 Indeed, microwave remote sensing is able to provide quantitative information about the water  
52 content of a shallow near surface layer (Schmugge, 1983), particularly in the low-frequency  
53 microwave region from 1 to 10 GHz. Passive microwave remote sensing of soil moisture has  
54 been at the center of attention of many research programs, for several decades. Various  
55 airborne and in situ radiometers have been developed, showing the high potential of L-band  
56 (1.41 GHz) measurements for the estimation of surface parameters (Skou, 1989, Wilson et al.,  
57 2001, Le Maitre et al., 2004). Whereas it was shown that surface soil moisture influences the  
58 microwave emission of relatively dense vegetation canopies from L-band to K-band (~1.41–  
59 23.8 GHz, e.g. Calvet et al., 2011), L-band is the optimal wavelength range to observe soil  
60 moisture (e.g. Wigneron et al., 1995). Higher frequencies are more significantly affected by  
61 perturbing factors such as atmospheric effects and vegetation cover (Schmugge, 1983, Kerr et  
62 al., 2001). At L-band, soil moisture in the first centimetres of soil impacts significantly on the  
63 emitted brightness temperature through a straightforward link between  $T_b$  and  $w_g$ , about 2 K  
64 per 1% of volumetric soil moisture over bare soil (Schmugge and Jackson, 1994, Chanzy et  
65 al., 1997).

66 From a satellite point of view, apart from a few days of L-band radiometric observations on  
67 Skylab between June 1973 and January 1974 (Jackson et al., 2004) current or past instruments  
68 have been operating at frequencies above 5 GHz. The Soil Moisture and Ocean Salinity  
69 mission (SMOS), is the first dedicated soil moisture mission launched in November 2009  
70 (Kerr et al., 2001, 2007). It consists of a spaceborne L-band (~1.42 GHz, 21 cm)  
71 interferometric radiometer using L-band radiometry able to provide multiangular microwave  
72 polarimetric brightness temperature ( $T_b$ ) and soil moisture product ( $w_g$ ). Wigneron et al.  
73 (1995, 2003), have shown that it is possible to retrieve biophysical variables from bipolarized  
74 and multiangular microwave  $T_b$ , including soil moisture. In the context of a validation  
75 campaign for the SMOS mission, the CAROLS L-Band (Cooperative Airborne Radiometer  
76 for Ocean and Land Studies) radiometer was designed, built and operated from an aircraft.  
77 The first CAROLS flights started in September 2007, for the qualification and certification of  
78 the instrument. Following various improvements to the CAROLS instrument, a second  
79 campaign was carried out in November 2008, in order to validate the CAROLS's data quality  
80 (Zribi et al., 2010). In the springs of 2009 and 2010, two scientific campaigns were organized,  
81 to acquire different types of brightness measurements over oceanic and land surfaces. This  
82 study focuses on land surface observations with several flights over the twelve stations of the  
83 SMOSMANIA (Soil Moisture Observing System – Meteorological Automatic Network  
84 Integrated Application) soil moisture network of Météo-France (Calvet et al., 2007, Albergel  
85 et al., 2008). SMOSMANIA consists in a long term data acquisition effort of profile soil  
86 moisture observations in southern France. The SMOSMANIA network was already used to  
87 assess soil moisture estimates from either remote sensing (Albergel et al., 2009) or numerical  
88 weather prediction models (Albergel et al., 2010). Additional in situ measurements were  
89 performed in 2009 and 2010, also, in three areas located within a SMOS pixel.

90 In this study, the two CAROLS campaigns of 2009 and 2010 over southwestern France are  
91 presented. The sensitivity of the CAROLS's  $T_b$  measurements to soil moisture is investigated.  
92 The  $T_b$  are compared to the in situ measurements of soil moisture, from the SMOSMANIA  
93 network and from the above mentioned additional measurements sites. Regressed empirical  
94 logarithmic equations are used to retrieve soil moisture from  $T_b$  observations. The retrieval  
95 performance of the regression (Calvet et al. 2011) is used as an indicator of the sensitivity of  
96 the CAROLS microwave to soil moisture and applied to SMOS data. After a description of  
97 the CAROLS airborne campaign and of the different soil moisture data sets used in this study,  
98 a short section describes the SMOS brightness temperatures. Then, a methodology for the  
99 evaluation the CAROLS data is presented, as well as the soil moisture retrieval method.  
100 Finally, the results are presented and discussed.

101

## 102 **2. Material and methods**

### 103 **2.1. CAROLS observations**

#### 104 **2.1.1. Flight description**

105 During the two scientific campaigns of springs 2009 and 2010, the CAROLS instrument  
106 onboard the research ATR-42 aircraft (Zribi et al. 2011), acquired L-band  $T_b$  (in conjunction  
107 with other measurements like infrared temperature) over the SMOSMANIA network, in  
108 southwestern France. Twenty-four flights were performed, at 2000m above sea level (asl): 6  
109 in 2009 and 18 in 2010. For some of them, manual measurements of soil moisture were made,  
110 in addition to the automated measurements of the SMOSMANIA network. Table 1 provides  
111 details of the two CAROLS campaign flights and Fig. 1 shows an overview of the flights. The  
112 studied flights covered either the whole transect over the SMOSMANIA network or the  
113 western part of the transect. The latter corresponded to ocean flights over the gulf of Biscay.

114 All the flights started from Toulouse, and observations were made from Toulouse to the gulf  
115 of Biscay and vice versa. The complete SMOSMANIA flights included an additional flight  
116 line from Toulouse to the Mediterranean sea and vice versa. A complete SMOSMANIA flight  
117 was performed in about 3 hours.

### 118 **2.1.2. CAROLS L-band radiometric observations**

119 CAROLS is a total power radiometer and has a simple structure and high theoretical  
120 sensitivity. The receiver was developed as a copy of the EMIRAD II radiometer, in  
121 collaboration between the DTU (Danish Technical University) and LATMOS (Laboratoire  
122 Atmosphères, Milieux, Observations Spatiales) laboratory. It is a fully polarimetric  
123 correlation radiometer using direct sampling, performing biangular ( $34^{\circ}$ - $0^{\circ}$ ) and bipolarized  
124 (V and H polarizations) observations. Two antennas provide dual-incidence measurements,  
125 useful for the estimation of soil moisture (Wigneron et al., 2004) or ocean salinity from  
126 brightness temperatures. The microwave emission of the surface is observed at two incidence  
127 angles, nadir ( $0^{\circ}$ ) and  $34^{\circ}$  (slant side-looking antenna). Considering a flight height of about  
128 2000m asl, the antenna spotting at nadir observes an area of 1362m large and the side looking  
129 antenna observes an area of 2062m large. In this configuration, given the simple straight-line  
130 flights at 2000m asl and the overlaid of both nadir and side looking antenna, the CAROLS  
131 instrument observes a corridor of about 3km, presented in Fig. 2. More information is  
132 available in Zribi et al. (2011). The radiometer was installed in the French research ATR-42  
133 aircraft in conjunction with other airborne instruments (C-Band scatterometer (STORM), the  
134 GOLD-RTR GPS system, the Infrared CIMEL radiometer and a visible wavelength camera).  
135 The CAROLS radiometer was validated and qualified with laboratory measurements (Zribi et.  
136 al., 2011). The infrared radiometer is part of the standard equipment of the research ATR-42.  
137 This instrument points to nadir, and has a  $3^{\circ}$  field of view. It measures the thermal emission

138 of the Earth's surface in three channels, 8.7, 10.8 and 12  $\mu\text{m}$ , respectively. It is used to  
139 provide surface temperature estimations, simultaneously with the CAROLS measurements.  
140 Radio Frequency Interferences (RFI) were observed by CAROLS along the SMOSMANIA  
141 transect (Zribi et al., 2011 ; Pardé et al., 2011). Passive radiometers are particularly  
142 susceptible to artificial microwave emissions (Njoku et al., 2005). The main sources  
143 responsible for most of the RFI were identified (Pardé et al. 2011). They correspond to  
144 antennas with an emission frequency within or spilling into the protected L-band used by both  
145 CAROLS and SMOS instruments. The identified RFI areas were suppressed from the data  
146 used in this study, as in Zribi et al. (2011). However, residual low RFI perturbations may  
147 remain in the data set.

## 148 **2.2. *In situ soil moisture: the SMOSMANIA network and*** 149 ***manual measurements***

150 The main objective of the SMOSMANIA network is to validate remotely sensed soil  
151 moisture. However the use of observations obtained from SMOSMANIA is not limited to  
152 satellite validation and other objectives include: (i) the validation of the operational soil  
153 moisture products of Météo-France, produced by the hydrometeorological SIM model  
154 (Habets et al., 2005, 2008), (ii) the validation of new versions of the ISBA land surface model  
155 of Météo-France, (iii) ground-truthing of airborne Cal/Val campaigns in support of the SMOS  
156 mission and (iv) the evaluation of remotely sensed soil moisture products.

157 The SMOSMANIA network is based on the existing automatic weather station network of  
158 Météo-France (RADOME, Réseau d'Acquisition de Données d'Observations  
159 Météorologiques Etendues). In 2006, twelve stations of the RADOME network in  
160 Southwestern France were equipped with soil moisture probes at four depths (5, 10, 20 and 30  
161 cm). The RADOME stations observe air temperature and relative humidity, wind speed and



162 precipitation. Downwelling shortwave radiation is also measured at some stations. The twelve  
163 stations of the SMOSMANIA network are located along a 400 km transect between the  
164 Mediterranean Sea and the Atlantic Ocean following the climatic gradient between the two  
165 coastlines. The three most westward and the three most eastward stations are located in areas  
166 with a high fraction of forests, either temperate or Mediterranean, respectively. The six  
167 stations at the centre of the transect, Peyrusse-Grande, Condom, Lahas, Savenes, Montaut,  
168 and Saint-Félix de Lauragais (PRG, CDM, LHS, SVN, MNT, and SFL, respectively), are  
169 located in areas dominated by croplands. The soil moisture measurements are in units of  
170  $\text{m}^3\text{m}^{-3}$ , they are derived from capacitance probes: ThetaProbe ML2X of Delta-T Devices,  
171 easily interfaced with the RADOME stations. A ThetaProbe provides a signal in units of volt  
172 and its variations is virtually proportional to changes in the soil moisture content over a large  
173 dynamic range (White et al., 1994). In this study, in order to convert the voltage signal into a  
174 volumetric soil moisture content, site-specific calibration curves were developed using in situ  
175 gravimetric soil samples, for each station, and each depth i.e., 48 calibrations curves (Calvet  
176 et al., 2007; Albergel et al., 2008). The ThetaProbes were installed in 2006 and have produced  
177 continuous observations since then, with a sampling time of 12 min. In this study, data  
178 acquired in 2010 are used. Along with soil moisture measurements, soil temperature is  
179 measured, also.

180 While SMOSMANIA was mainly designed to support the validation of soil moisture  
181 estimates from SMOS, other satellite-derived surface soil moisture products may be  
182 considered, together with model soil moisture estimates over France (Rüdiger et al., 2009;  
183 Albergel et al., 2009, 2010), e.g. AMSR-E (Advanced Microwave Scanning Radiometer for  
184 Earth Observing System), WindSAT (a multi-frequency polarimetric microwave radiometer),  
185 or the C-band ASCAT (Advanced Scatterometer) instrument. Figure 1 shows the  
186 SMOSMANIA network in southwestern France. The Lézignan-Corbières (LZC) station is not

187 used in this study as no data were observed for most of the 2010 period due to technical  
188 problems.

189 In addition to the twelve stations of the SMOSMANIA network, soil moisture was measured  
190 at three transects within an area representative of a SMOS pixel, at the east of the LHS  
191 station. These observations were performed in order to characterize the heterogeneity of the  
192 pixel. The transects are presented in Fig. 3. The first one (Le Mona) is representative of an  
193 hilly agricultural area with mixed crops, the second one (Lahage) corresponds to a forest and  
194 the third one (Berat) is a flat agricultural area with maize. Soil moisture was sampled within  
195 the three sites, under the flight track in conjunction with the CAROLS flights. Measurements  
196 were performed using Thetaprobes, as used for the the SMOSMANIA stations, providing a  
197 signal in units of volt. A calibration curve was developed to convert the voltage into  
198 volumetric soil moisture content ( $\text{m}^3\text{m}^{-3}$ ). The calibration was performed in situ through  
199 regular gravimetric samples over the three sites. 90 gravimetric measurements were acquired  
200 in 2009 allowing the determination of a calibration curve with an accuracy of about 0.03  
201  $\text{m}^3\text{m}^{-3}$ . Figure 4 presents an illustration of the soil moisture data sampled at the Le Mona site  
202 for 28 April 2010.

### 203 **2.3. SMOS brightness temperatures**

204 Brightness temperature and soil moisture from SMOS mission are also used in this study. One  
205 of the main objectives of SMOS is the mapping of global surface soil moisture with an  
206 accuracy better than  $0.04 \text{ m}^3 \text{ m}^{-3}$ , every three days (Kerr et al., 2001). The 2-D interferometric  
207 radiometer allows measuring  $T_b$  at many incidence angles, and is fully polarized. Over land  
208 surfaces, the sensitivity of individual SMOS  $T_b$  observations at a given location ranges  
209 between 2.5 and 4K. While such high noise levels are detrimental to soil moisture retrieval  
210 (Pellarin et al. 2003a), the use of several  $T_b$  values, at two polarizations and for several  
211 incidence angles, permits to cope with this problem.

212 In this study, the  $T_bV$  and  $T_bH$  at an incidence angle of  $34^\circ$  (consistent with the incidence  
213 angle of the  $T_b$  observed by the CAROLS slant antenna) were extracted for the different  
214 studied sites, from L1c SMOS product provided to CAL/VAL teams by ESA. They  
215 corresponded to data before any reprocessing, i.e., with faults in the calibration and  
216 inconsistencies in the processing (due to the commissioning phase activities). Results are thus  
217 to be considered with caution. Valid SMOS observations close to nadir were scarce, and  $T_b$   
218 values at  $34^\circ$  were considered, only. First, the  $T_b$  were corrected for the Faraday rotation  
219 induced by the ionosphere and recalculated from the antenna (X, Y polarizations) to the Earth  
220 surface (H and V polarizations) reference frame. Second,  $T_bV$  and  $T_bH$  median values were  
221 calculated in a range of incidence angles of  $34^\circ \pm 2^\circ$ . The SMOS observations over France  
222 are subjected to RFI, and in southwestern France, the most affected area is the Atlantic part of  
223 the CAROLS transect. In order to remove contaminated measurements, the data were filtered.  
224 The filter criterion used for SMOS  $T_b$  was based on halved first Stokes parameter calculated  
225 as  $T_bS1 = 0.5 * (T_bH + T_bV)$  (Kerr et al., 2007). The  $T_b$  measurements out of a two standard  
226 deviation interval were considered to be contaminated by RFI. The mean value and standard  
227 deviation of  $T_bS1$  were calculated for the March-July 2010 period over the France domain.

## 228 **2.4. Methodology**

229 For each station of the SMOSMANIA network, CAROLS  $T_b$  are averaged within a 20 km  
230 radius around the station, consistent with the scale of a SMOS pixel ( $\sim 40$  km), and compared  
231 to soil moisture observations. When considering the 3 additional sites, they are averaged  
232 within a 1 km radius to be compared with in situ observations and within 20 km to be  
233 compared with the soil moisture as seen by SMOS. Retrieving soil moisture from microwave  
234  $T_b$ , Wigneron et al. (2004) have shown that the  $\tau$ - $\omega$  model (Wigneron et al., 1995) can be used  
235 to build semi-empirical statistical relationships between  $w_g$  and microwave reflectivities  
236 observed at two contrasting incidence angles. These relationships could, potentially, be used

237 for  $w_g$  and vegetation optical thickness retrieval. Saleh et al. (2006), presented a review of  
 238 index-based methods and semi-empirical regression methods at L-band. They consist of either  
 239 single configurations (one incidence angle, one polarization) or multiple configurations (one  
 240 polarization and two angles, or two polarizations and one angle). Saleh et al. (2006)  
 241 demonstrated that better  $w_g$  retrievals are obtained with the multiple configuration regression  
 242 (either biangular or bipolarization). In addition to soil moisture, it is possible to retrieve the  
 243 vegetation water content (VWC) and the optical depth of the canopy (which depends on the  
 244 VWC). This study focuses on  $w_g$  retrieval, and the multiple configuration regression method  
 245 used to assess the sensitivity of the CAROLS's microwave observations to  $w_g$  at different  
 246 frequencies is presented by Eq.(1a). Eq.(1a) was used by Calvet et al. (2011), adapted from  
 247 Saleh et al. (2006).

$$248 \quad w_g = \exp\left( A_{w_g} \ln\left(1 - \frac{T_b(\theta_1, p)}{T_{IR}}\right) + B_{w_g} \ln\left(1 - \frac{T_b(\theta_2, q)}{T_{IR}}\right) + c_{w_g} \right) \quad \text{Eq.(1a)}$$

249 Eq.(1a) is used with CAROLS data in three configurations, two biangular ( $\theta_1 \neq \theta_2$ ,  $p=q$ , i.e.  
 250 34H0H and 34V0V) and one bipolarized ( $\theta_1 = \theta_2$ ,  $p \neq q$ , i.e. 34VH) configurations. Following  
 251 Saleh et al. (2006), the regression coefficients  $A_{w_g}$ ,  $B_{w_g}$ ,  $C_{w_g}$  may vary from one configuration  
 252 to another. As in Calvet et al. (2011) the regression coefficients are based on  $w_g$  observations  
 253 from either the SMOSMANIA network or additional measurements,  $T_b$  and surface  
 254 temperature estimates. The use of the airborne infrared temperature observations ( $T_{IR}$ ) would  
 255 limit the analysis of the empirical coefficients to the CAROLS flight times. Indeed, the  
 256 availability of the SMOS data is not restricted to the CAROLS flight times. Therefore, an  
 257 effective temperature ( $T_{eff}$ ) based on the SMOSMANIA soil temperature profiles were used  
 258 instead of  $T_{IR}$ , for both CAROLS and SMOS  $T_b$ :

$$259 \quad w_g = \exp\left( A_{w_g} \ln\left(1 - \frac{T_b(\theta_1, p)}{T_{eff}}\right) + B_{w_g} \ln\left(1 - \frac{T_b(\theta_2, q)}{T_{eff}}\right) + c_{w_g} \right) \quad \text{Eq.(1b)}$$

260 The simple method of estimation of  $T_{\text{eff}}$  uses measured or simulated ground temperatures  
261 ( $T_{\text{gr}}$ ) at the different depth. The simple approach developed by Choudhury (Choudhury et al.,  
262 1982) to estimate  $T_{\text{eff}}$  consists of using two soil temperatures: at depth ( $T_{\text{depth}}$ ) and at the  
263 surface ( $T_{\text{surf}}$ ).

$$264 \quad T_{\text{eff}} = T_{\text{depth}} + (T_{\text{surf}} - T_{\text{depth}}) C_t \quad \text{Eq.(2)}$$

265 where  $C_t$  depends on frequency (L-band in this study). While Choudhury et al. (1982) use  $C_t$   
266 = 0.246 at L-band, Wigneron et al. (2008) developed and tested more complex formulations  
267 that account for the dependence of  $C_t$  on soil moisture and soil texture - clay and sand content.  
268 In this study, soil temperature values measured by the SMOSMANIA stations are used:  $T_{\text{surf}}$   
269 at 5cm and  $T_{\text{depth}}$  at 30 cm. As a preliminary analysis showed no significant added value of the  
270 most complex approaches on the results of this study, the results obtained using the simple  
271 Choudhury approach are shown, only. Moreover, it was checked (not shown) that the higher  
272  $C_t$  values given by Wigneron et al. (2008) for Eq. (2), ranging from 0.5 to 1, tend to reduce  
273 the number of usable  $T_b$  values in Eq. (1b), as  $T_{\text{eff}}$  values are higher. Finally,  $C_t = 0.246$  was  
274 used.

275 In a first attempt to test the sensitivity of CAROLS microwave observations to  $w_g$ , three  
276 scores are considered: the correlation ( $r$ ), the root mean square error (RMSE) and the Fisher's  
277  $F$ -test  $p$ -value. The  $p$ -value indicates the significance of the test, if it is small (e.g. below  
278 0.05), it means that the correlation is not a coincidence. In this study, the following thresholds  
279 on  $p$ -values are used: (i) NS (non significant) for  $p$ -value greater than 0.05, (ii) \* between  
280 0.05 and 0.01, (iii) \*\* between 0.01 and 0.001, (iv) \*\*\* between 0.001 and 0.0001 and (v)  
281 \*\*\*\* below a value of 0.0001.

282

283

## 284 **3. Results**

### 285 **3.1. Sensitivity of CAROLS $T_b$ to $w_g$**

286 As an illustration of the CAROLS  $T_b$  response to surface soil moisture, Fig. 5 presents  
287 CAROLS's microwave observations (dots) at nadir ( $0^\circ$ ) in vertical polarization (V) with  
288 errors bars (standard deviation) for two neighboring stations (less than 40 km apart) of the  
289 SMOSMANIA network. Precipitation is presented, also. On the basis of Fig. 5, it is possible  
290 to appreciate the response of  $T_b$  to rain events (i.e. to rises in surface soil moisture). The  
291 precipitation events correspond to reduced  $T_b$ , whereas the drying out following the  
292 precipitation events corresponds to increases in  $T_b$ . The strong link between L-band  $T_b$  and  $w_g$   
293 is demonstrated by Table 2, presenting the correlation between  $T_b$  (in four configurations,  
294 nadir and slant in both H and V polarization) and  $w_g$ . Regarding the SMOSMANIA network,  
295 scores are better with  $T_b$  at nadir, with correlations ranging from -0.526 to -0.878, at either  
296 vertical or horizontal polarization, with an average of -0.76.  $T_b$  at slant present lower  
297 correlations, ranging from -0.169 to -0.494 (with an average of -0.30) and -0.241 to -0.737  
298 (with an average of -0.58), at V and H polarization, respectively. For Le Mona, Lahage and  
299 Berat sites, average correlations greater than -0.82 are obtained (see Table 2), except for  
300 CAROLS  $T_b$  at slant ( $34^\circ$ ) V polarization which presents low correlations (-0.208 on  
301 average).

302 Figure 6 presents, for each station of the SMOSMANIA network, and for the three additional  
303 sites, the CAROLS microwave observations (nadir, V polarization) as a function of soil  
304 moisture for 2009 and 2010. More often than not, tendencies observed for both 2009 and  
305 2010 are similar. However, the Le Mona case is of interest. While  $T_b$  values observed in 2009  
306 are in the same range as those observed in 2010, the observed  $w_g$  were higher in 2009. Indeed,  
307 the L-band sensitivity to  $w_g$  depends on vegetation attenuation. In spring 2009, the Le Mona

308 site was covered by a dense rapeseed crop, whereas in 2010 it was covered by wheat  
309 (relatively sparse at this period of the year). This explains that despite higher  $w_g$  values in  
310 2009, the observed  $T_b$  are within the same range of the ones of 2010.

### 311 **3.2. From CAROLS $T_b$ to $w_g$ using a dual configuration** 312 **regression**

313 Table 3 presents the results obtained for the 34H0H, 34V0V and 34VH configurations with  
314  $T_{\text{eff}}$  estimated using the first Eq. (2) formulation. Figure 7 illustrates the results of the 34VH  
315 configuration. This configuration presents the best scores, with only three sites (of 14) with  
316 non significant  $p$ -values ( $>0.05$ ). These three sites correspond to forested areas, in the Les  
317 Landes forest (SBR site) and in a hilly area of Corbières (MTM). Regarding stations with  
318 significant statistical scores, the correlations and RMSE scores range from 0.50 to 0.93 and  
319 from 0.015 to 0.044  $\text{m}^3\text{m}^{-3}$ , respectively. For 34H0H, the correlations tend to be lower than  
320 for 34VH, for several stations. Moreover, the use of the biangular configuration is limited for  
321 two stations close to strong RFI zones, PRG and CDM, which are affected by residual  
322 interferences, as shown by the high fraction of missing data for these two stations (Table 2):  
323 84% and 77%, respectively, against an average value of 49% for all the stations. Indeed, the  
324 nadir  $T_b$  at these stations are often higher than  $T_{\text{eff}}$ , and this can be explained by residual RFI  
325 levels. Only 4 flights for CRD site and 6 flights for CDM site are found to be suitable to  
326 produce the score. This is not enough to obtain significant regressions. The 34V0V  
327 configuration is the less efficient, with six sites presenting non-significant correlations.

328 Table 4 presents the  $A_{wg}$ ,  $B_{wg}$  and  $C_{wg}$  regression coefficient values of the dual-configuration  
329 regression method used in this study. They vary from a configuration to another and seem to  
330 be site specific. They may depend on the soil and vegetation properties acting on the  
331 microwave emission, like soil roughness, surface infiltration and thermal properties,

332 vegetation phenology and canopy structure. Observed soil characteristics such as organic  
333 matter, clay and sand fractions, bulk density, are available for SMOSMANIA (Albergel et al.,  
334 2008). The link between the  $A_{wg}$ ,  $B_{wg}$  and  $C_{wg}$  regression coefficients and the above mentioned  
335 characteristics was investigated (not shown). However no significant link between regressions  
336 coefficient and soil characteristics could be established.

### 337 **3.3. Application to SMOS brightness temperatures**

338 The  $A_{wg}$ ,  $B_{wg}$  and  $C_{wg}$  regression coefficients determined for CAROLS's measurements were  
339 applied to these SMOS  $T_b$  data previously filtered for RFI. The scores between the retrieved  
340  $w_g$  from SMOS and observed soil moisture are presented in Table 5. For eight stations of the  
341 SMOSMANIA network the correlations are significant ( $p$ -value  $<0.05$ ) with  $r$  and RMSE  
342 ranging from 0.25 to 0.60 and from 0.03 to 0.09  $m^{-3}m^{-3}$ , respectively. The best scores ( $p$ -value  
343  $<0.001$ ) are obtained for SBR, MNT, and SFL (Fig. 8). Correlations are significant for the Le  
344 Mona, Lahage and Berat sites, also. The average RMSE value for all the significant  
345 correlations is  $0.06m^{-3}m^{-3}$  which is similar to the RMSE obtained with the ASCAT surface  
346 soil moisture products over the same sites (Albergel et al. 2009).

## 347 **4. Discussion**

348 This study investigated the sensitivity of CAROLS's L-band  $T_b$  to soil moisture, over various  
349 landscape types. The dual configuration regression method used by Calvet et al. (2011) to  
350 assess the sensitivity to soil moisture was applied to the CAROLS biangular and bipolarized  
351 observations. The regression coefficients obtained for the 34VH configuration were applied to  
352 the SMOS  $T_b$ , also. The results obtained over three sites URG, LHS and SVN (Table 5) show  
353 no sensitivity to soil moisture (non-significant correlations). However, Albergel et al. (2009)  
354 and Albergel et al. (2010), found good correlations between in situ surface soil moisture  
355 observations at these sites and the ASCAT product. The lack of consistency between the



356 SMOS and the ASCAT or CAROLS results over some SMOSMANIA sites may be explained  
357 by:

- 358 • scale issues inducing discrepancies between the environment of the local in situ  
359 observations and the area of the size of a SMOS footprint around them,
- 360 • the presence of residual RFI in the SMOS  $T_b$  dataset,
- 361 • the fact that the SMOS data are not reprocessed,
- 362 • the need to include more information into the regression equation (e.g. besides two  
363 polarizations, several contrasting incidence angles ; ancillary information about the  
364 vegetation opacity).

365 Whereas Saleh et al. (2010) suggested that the  $A_{wg}$ ,  $B_{wg}$  and  $C_{wg}$  regression coefficients may  
366 depend on soil and vegetation characteristics, no significant link between regression  
367 coefficients and measured soil characteristics (such as soil texture, organic matter content, or  
368 dry density) could be established using the SMOSMANIA network. It must be noted that soil  
369 roughness (not measured) impacts  $T_b$ , also. The purpose of the manual measurements  
370 performed at Le Mona, Lahage, and Berat sites (close to the LHS SMOSMANIA station),  
371 was to test the representativeness of local observations. While the results presented in Fig. 7  
372 show that soil moisture observations at these four sites are in the same range, the coefficients  
373 of the regressions Eq. (1b) markedly differ from one site to another (Table 3), in relation to  
374 contrasting vegetation, soil and relief characteristics. In particular, the Berat agricultural site  
375 presents a lower correlation than the other sites. Indeed, it is less representative of the area  
376 where distributed in situ measurements were taken, as it consisted of large flat maize fields  
377 with mainly bare soil in April and May, and rapidly growing maize in June.

378 Finally, as the coefficients of Eq. (1b) are derived from  $T_b$  observations obtained at various  
379 dates, they implicitly represent the average vegetation impact on  $T_b$  and the seasonal variation  
380 of vegetation properties, e.g. the vegetation water content (not measured). A consequence of

381 the latter effect is that the values for the regression coefficients should not only be site  
382 specific but also show seasonal variation if computed separately for the main seasons. It is  
383 likely that the limited number of sites does not allow a robust analysis of the regression  
384 coefficients, and a modeling study with the version of the ISBA model able to simulate  
385 vegetation growth (Calvet et al. 1998) could help investigating this issue.

386 Correlations between CAROLS  $T_b$  and in situ soil moisture are generally higher at nadir than  
387 at slant. A number of factors may explain this result. In particular, the area spotted by  
388 CAROLS at nadir is smaller than the one spotted at slant, and more representative of the in  
389 situ observations. Also, nadir observations are less affected by the vegetation opacity. Except  
390 for the PRG and CDM stations, presenting nadir observations affected by RFI, the Eq. (1b)  
391 regression using data at  $34^\circ$  at both polarizations yields results similar to the regressions using  
392 two angles at only one polarization. This is consistent with the results of Calvet et al. (2011),  
393 showing similar L-band soil moisture retrieval scores with one angle and two polarizations  
394 (30VH or 40VH), and two angles and one polarization (50V20V, 40V20V, 50H20H,  
395 40H20H).

396 In addition to the RFI issue, the signal is influenced by the vegetation. A reduced sensitivity  
397 to soil moisture is to be expected over dense vegetation canopies. However, some stations,  
398 characteristic of highly vegetated agricultural areas (e.g. MNT) present very good scores. A  
399 possible explanation could be the presence of a significant fraction of bare soil and/or dry  
400 vegetation, caused by the crop rotation practices. This factor may explain the significant  
401 response of  $T_b$  to soil moisture observed over agricultural areas, at L-band and, also, at higher  
402 frequencies (Calvet et al., 2011).

403 Regarding the SMOS data, two levels of products are distributed, brightness temperatures and  
404 soil moisture derived from the brightness temperatures. The soil moisture retrieval method is  
405 based on the  $\tau$ - $\omega$  model associated to a soil emission model, inverted through optimization

406 methods (Pellarin et al. 2003a). This study confirms that simple regression methods (Pellarin  
407 et al. 2003b) are able to produce satisfactory results over a given set of sites. Even if  $A_{wg}$ ,  $B_{wg}$   
408 and  $C_{wg}$  regression coefficients seem to be site specific, the triplets of coefficients derived  
409 from the CAROLS data were successfully applied to the SMOS brightness temperatures.  
410

## 411 **5. Conclusions**

412 This study provides several insights into the sensitivity to soil moisture of passive microwave  
413 observations at L-band. The performance of simple logarithmic statistical regression  
414 equations relating  $w_g$  to the microwave emissivity was used as an indicator of this sensitivity.  
415 The CAROLS L-band observations were found to be very sensitive to soil moisture in the  
416 different configurations tested. Once converted to  $w_g$  using simple logarithmic statistical  
417 regression equations, the retrieved  $w_g$  present good correlations with observations. The  
418 application of the regression coefficients determined from the CAROLS emissivities to the  
419 SMOS emissivities showed promising results and a more in-depth analysis of this method is  
420 needed. The use of CAROLS L-band measurements and their confrontation to observed soil  
421 moisture is a first step before the evaluation of the SMOS products, to be reiterated when  
422 future reprocessed data become available.

423

424

## 425 **Acknowledgements**

426 The work of C. Albergel was supported by Centre National d'Etudes Spatiales (CNES) and  
427 Météo-France. The work of E. Zakharova was supported by the STAE (Sciences et  
428 Technologies pour l'Aéronautique et l'Espace) foundation, in the framework of the CYMENT  
429 project. The CAROLS project was funded by the "Programme Terre Océan Surface

430 Continentales et Atmosphère” (TOSCA, CNES). The ATR-42 aircraft was operated by the  
431 SAFIRE UMS 2859.

432

433

## 434 **References**

- 435 Albergel, C., Rüdiger, C., Pellarin, T., Calvet, J.-C., Fritz, N., Froissard, F., Suquia, D.,  
436 Petitpa, A., Piguet, B., & Martin, E. (2008). From near-surface to root-zone soil  
437 moisture using an exponential filter: an assessment of the method based on in-situ  
438 observations and model simulations. *Hydrol. Earth Syst. Sci.*, *12*, 1323–1337.  
439 doi:10.5194/hess-12-1323-2008.
- 440 Albergel, C., Calvet, J.-C., de Rosnay, P., Balsamo, G., Wagner, W., Hasenauer, S., Naemi,  
441 V., Martin, E., Bazile, E., Bouyssel, F., & Mahfouf, J.-F. (2010). Cross-evaluation of  
442 modelled and remotely sensed surface soil moisture with in situ data in southwestern  
443 France, *Hydrol. Earth Syst. Sci.*, *14*, 2177-2191. doi:10.5194/hess-14-2177-2010.
- 444 Albergel, C., Rüdiger, C., Carrer, D., Calvet, J.-C., Fritz, N., Naeimi, V., Bartalis, Z., &  
445 Hasenauer, S. (2009). An evaluation of ASCAT surface soil moisture products with in-  
446 situ observations in southwestern France. *Hydrol. Earth Syst. Sci.*, *13*, 115-124.  
447 doi:10.5194/hess-13-115-2009.
- 448 Calvet, J.-C., Noilhan, J., Roujean, J.-L., Bessemoulin, P., Cabelguenne, M., Olioso, A., &  
449 Wigneron, J.-P. (1998). An interactive vegetation SVAT model tested against data from  
450 six contrasting sites. *Agric. For. Meteorol.*, *92*, 73–95, 1998.
- 451 Calvet, J.-C., Fritz, N., Froissard, F., Suquia, D., Petitpa, A., & Piguet, B. (2007). In situ soil  
452 moisture observations for the CAL/VAL of SMOS: the SMOSMANIA network.  
453 *Proceedings of the International Geoscience and Remote Sensing Symposium, IGARSS*,  
454 Barcelona. doi: 10.1109/IGARSS.2007.4423019.
- 455 Calvet, J.-C., Wigneron, J.-P., Walker, J., Karbou, F., Chanzy, A., & Albergel, C. (2011).  
456 Sensitivity of passive microwave observations to soil moisture and vegetation water  
457 content: L-band to W band. *IEEE Trans. Geosci. Remote. Sens.*, *49*(4), 1190 – 1199, doi  
458 :10.1109/TGRS.2010.2050.488.

459 Chanzy, A., Schmugge, T. J., Calvet, J.-C., Kerr, Y., van Oevelen, P., Grosjean, O., & Wang,  
460 J.R. (1997). Airborne microwave radiometry on a semi arid area during Hapex-sahel. *J.*  
461 *Hydrol.*, 188-189, 285-309.

462 Choudhury, B. J., Schmugge, T. J., & Mo, T. (1982). A parameterization of effective soil  
463 temperature for microwave emission. *J. Geophys. Res.*, 87, C2, 1301–1304.

464 Dirmeyer, P.A., Dolman, A.J., & Sato, N. (1999). The pilot phase of the global soil wetness  
465 project. *Bull. Amer. Meteorol. Soc.*, 80, 851-878.

466 Georgakakos, K.P., & Carpenter, M. (2006). Potential value of operationally available and  
467 spatially distributed ensemble soil water estimates for agriculture. *J. Hydrol.*, 328, 177-  
468 191.

469 Habets, F., Ducrocq, V., & Noilhan, J. (2005). Prévisions hydrologiques et échelles spatiales:  
470 l'exemple des modèles opérationnelles de Météo-France, *C. R. Geoscience*, 337, 181–  
471 192.

472 Habets F., Boone, A., Champeaux, J.-L., Etchevers, P., Franchisteguy, L., et al. (2008). The  
473 SAFRAN-ISBA-MODCOU hydrometeorological model applied over France, *J.*  
474 *Geophys. Res.*, 113, D06113, doi:10.1029/2007JD008548.

475 Jackson, T.J., Hsu, A.Y., van de Griend, A., & Eagleman, J.R. (2004). Skylab L band  
476 microwave radiometer observations of soil moisture revisited, *Int. J. Remote Sens.*, 25,  
477 2585-2606.

478 Kerr, Y., Waldteufel, P., Wigneron, J.-P., Martinuzzi, J.-M., Font, J., & Berger, M. (2001).  
479 Soil moisture retrieval from space: the soil moisture and ocean salinity (SMOS) mission,  
480 *IEEE Trans. Geosci. Remote. Sens.*, 39, 1729–1736.

481 Kerr Y., Waldteufel, P., Richaume, P., Davenport, I., Ferrazzoli, P., & Wigneron, J.-P.  
482 (2007). SMOS level 2 processor soil moisture algorithm theoretical basis document

483 (ATBD), CESBIO, Toulouse, France. SM-ESL (CBSA), SO-TN-ESL-SM-GS-0001,  
484 ESA Internal report, V2.a., <http://www.cesbio.ups-tlse.fr/us/indexsmos.html>

485 Kerr, Y. (2007). Soil moisture from space: where are we? *Hydrogeol. J.*, *15*(1), 117–120.

486 Lemaître, F., Poussière, J. K., Kerr, Y. H., Déjus, M., Durbe, R., De Rosnay, P., & Calvet, J.-  
487 C. (2004). Design and test of the ground based L-band radiometer for estimating water  
488 in soils (LEWIS). *IEEE Trans. Geosci. Remote. Sens.*, *42*, 8, 1666-1676.

489 Njoku, E. G., Jackson, T. J., Lakshmi, V., Chan, T. K., & Nghiem, S. V. (2003). Soil moisture  
490 retrieval from AMSR-E, *IEEE Trans. Geosci. Remote. Sens.*, *41*(2), 215–123.

491 Njoku, E. G., Ashcroft, P., Chan, T. K., & Li, L. (2005). Global survey and statistics of radio-  
492 frequency interference in AMSR-E land observations, *IEEE Trans. Geosci. Remote.*  
493 *Sens.*, *43*, 938-947.

494 Pardé, M., Zribi, M., Fanise, P., & Dechambre, M. (2011). Analysis of RFI issue using the  
495 CAROLS L-band experiment, *IEEE Trans. Geosc. Remote Sens.*, *49* (3), 1063-1070.

496 Pellarin, T., Wigneron, J.-P., Calvet, J.-C., & Waldteufel, P. (2003a). Global soil moisture  
497 retrieval from a synthetic L-band brightness temperature data set. *J. Geophys. Res.*, *108*,  
498 *D12*, 4364. doi : 10.1029/2002JD003086.

499 Pellarin, T., Calvet, J.-C., & Wigneron, J.-P. (2003b). Surface Soil Moisture Retrieval from L-  
500 band radiometry: a Global Regression Study. *IEEE Trans. Geosc. Remote Sens.*, *41*, 9,  
501 2037-2051.

502 Rüdiger, C., Calvet, J.-C., Gruhier, C., Holmes, T., De Jeu, R., & Wagner, W. (2009). An  
503 intercomparison of ERS-Scat and AMSR-E soil moisture observations with model  
504 simulations over France. *J. Hydrometeorol.*, *10*(2), 431–447.  
505 doi:10.1175/2008JHM997.1

506 Saleh, K., Wigneron, J.-P., de Rosnay, P., Calvet, J.-C., & Kerr, Y. (2006). Semi empirical  
507 regression s at L-Band applied to surface soil moisture retrieval over grass. *Remote*  
508 *Sens. Environ.*, *101* (3), 415-426.

509 Schmugge, T. J. (1983). Remote sensing of soil moisture: recent advances, *IEEE Trans.*  
510 *Geosc. Remote Sens.*, *GE21*, 145–146.

511 Schmugge, T. J., & Jackson, T.J. (1994). Mapping soil moisture with microwave radiometers,  
512 *Meteorol. Atmos. Phys.*, *54*, 213-223.

513 Skou, N. (1989). Microwave radiometer systems: design and analysis. MA, Norwood, USA:  
514 Artech House.

515 Wagner, W., Lemoine, G., & Rott, H. (1999). A method for estimating soil moisture from  
516 ERS scatterometer and soil data. *Remote Sens. Environ.*, *70*, 191-207.

517 Wagner, W., Naeimi, V., Scipal, K., de Jeu, R., & Martinez-Fernandez, J. (2007). Soil  
518 moisture from operational meteorological satellites, *Hydrogeol. J.*, *15*, 121–131.

519 Wagner, W., Blöschl, G., Pampaloni, P., Calvet, J.-C., Bizzarri, B., Wigneron, J.-P., & Kerr,  
520 Y. (2007). Operational readiness of microwave remote sensing of soil moisture for  
521 hydrologic applications. *Nord. Hydrol.*, *38*(1), 1–20. doi:10.2166/nh2007.029.

522 White, I., Knight, J. H., Zegelin, S. J., & Topp, G. C. (1994). Comments on “Considerations  
523 on the use of time-domain reflectometry (TDR) for measuring soil water content”, by  
524 Whalley, W. R., Response, *Eur. J. Soil Sci.*, *45*(4), 503–510.

525 Wigneron, J.-P., Chanzy, A., Calvet, J.-C., & Bruguier, N. (1995). A simple algorithm to  
526 retrieve soil moisture and vegetation biomass using passive microwave measurements  
527 over crop fields. *Remote Sens. Environ.*, *51* (3), 331-341.

528 Wigneron, J.-P., Calvet, J.-C., Pellarin, T., Van de Griend, A., Berger, M., & Ferrazzoli, P.  
529 (2003). Retrieving near surface soil moisture from microwave observations: Current  
530 status and future plan. *Remote Sens. Environ.*, *85*, (4), 489-506.



531 Wigneron, J.-P., Calvet, J.-C., de Rosnay, P., Kerr, Y., Waldteufel, P., Saleh, K., Escorihuela,  
532 M.J., & Kruszewski, A. (2004). Soil moisture retrievals from biangular L-Band passive  
533 microwave observations, *IEEE Geosci. Remote Sens. Lett.*, *1* (4), 277-281.

534 Wigneron, J.-P., Chanzy, A., de Rosnay, P., Rüdiger, C., & Calvet, J.-C. (2008). Estimating  
535 the effective soil temperature at L-band as a function of soil properties, *IEEE Trans.*  
536 *Geosc. Remote Sens.*, *46* (3), 797-801.

537 Wilson, W. J., Yueh, S. H., Dinardo, S. J., Chazanoff, S. L., Kitiyakara, A., Li, F. K., &  
538 Rahmat-Samii, Y. (2001). Passive active L- and S-Band (PALS) microwave sensor for  
539 ocean salinity and soil moisture measurements, *IEEE Trans. Geosc. Remote Sens.*, *39*, 5,  
540 1039-1048.

541 Zribi, M., Pardé, M., Boutin, J., Fanise, P., Hauser, D., Dechambre, M., Kerr, Y., Leduc-  
542 Leballeur, M., Skou, M., Søbjaerg, S.S., Albergel, C., Calvet, J.-C., Wigneron, J.-P.,  
543 Lopez-Baeza, E., Ruis, A., & Tenerelli, J. (2011). CAROLS: a new airborne L-band  
544 radiometer for ocean surface and land observations. *Sensors*, *11*, 719-742.  
545 doi:10.3390/s110100719.

546

547 **Tables**

548

549 Table 1: Description of the 24 flights (6 in 2009 and 18 in 2010) performed during the  
 550 CAROLS campaigns and taken in consideration in this study. Other flights performed over  
 551 Spain are not used here.

| Date          | Flight plan        | Additional in situ measurements |
|---------------|--------------------|---------------------------------|
| 2009 April 28 | SMOSMANIA transect | YES                             |
| 2009 May 15   | SMOSMANIA transect | YES                             |
| 2009 May 18   | Gulf of Biscay     | NO                              |
| 2009 May 20   | Gulf of Biscay     | NO                              |
| 2009 May 26   | Gulf of Biscay     | NO                              |
| 2009 May 27   | SMOSMANIA transect | YES                             |
| 2010 April 15 | SMOSMANIA transect | YES                             |
| 2010 April 28 | SMOSMANIA transect | YES                             |
| 2010 May 03   | SMOSMANIA transect | NO                              |
| 2010 May 06   | Gulf of Biscay     | NO                              |
| 2010 May 08   | Gulf of Biscay     | NO                              |
| 2010 May 09   | SMOSMANIA transect | NO                              |
| 2010 May 11   | Gulf of Biscay     | NO                              |
| 2010 May 19   | Gulf of Biscay     | NO                              |
| 2010 May 21   | SMOSMANIA transect | NO                              |
| 2010 May 26   | SMOSMANIA transect | YES                             |
| 2010 May 31   | SMOSMANIA transect | NO                              |
| 2010 June 04  | SMOSMANIA transect | NO                              |
| 2010 June 08  | SMOSMANIA transect | YES                             |
| 2010 June 13  | SMOSMANIA transect | NO                              |
| 2010 June 18  | SMOSMANIA transect | YES                             |
| 2010 June 22  | SMOSMANIA transect | NO                              |
| 2010 June 26  | SMOSMANIA transect | NO                              |
| 2010 July 01  | SMOSMANIA transect | YES                             |

552

553

554 Table 2: Correlations between CAROLS  $T_b$  (in four configurations, nadir and slant antennas,  
555 at both H and V polarization) and  $w_g$  using the pooled 2009-2010 data set. The fraction of  
556 data removed from the analysis (of the 2010 flights), as suspected to be contaminated by  
557 radio-frequency interferences, is indicated (right column).

| Station        | CAROLS $T_b$ at nadir ( $0^\circ$ ) |               |    | CAROLS $T_b$ at $34^\circ$ |               |    | Fraction of missing data (%) |
|----------------|-------------------------------------|---------------|----|----------------------------|---------------|----|------------------------------|
|                | V pol.                              | H pol.        | N  | V pol.                     | H pol.        | N  |                              |
| SBR            | -0,526                              | -0,529        | 24 | -0,338                     | -0,241        | 24 | 69                           |
| URG            | -0,754                              | -0,738        | 24 | -0,269                     | -0,660        | 24 | 34                           |
| CRD            | -0,810                              | -0,760        | 24 | -0,198                     | -0,495        | 24 | 31                           |
| PRG            | -0,867                              | -0,865        | 24 | -0,240                     | -0,737        | 24 | 84                           |
| CDM            | -0,780                              | -0,878        | 24 | -0,299                     | -0,610        | 24 | 77                           |
| LHS            | -0,728                              | -0,724        | 24 | -0,233                     | -0,545        | 24 | 34                           |
| SVN            | -0,805                              | -0,814        | 24 | -0,169                     | -0,523        | 24 | 36                           |
| MNT            | -0,870                              | -0,862        | 22 | -0,410                     | -0,655        | 22 | 36                           |
| SFL            | -0,730                              | -0,728        | 17 | -0,361                     | -0,701        | 18 | 39                           |
| MTM            | -0,691                              | -0,667        | 17 | -0,494                     | -0,606        | 18 | 48                           |
| LZC            | /                                   | /             | /  | /                          | /             | /  | 52                           |
| NBN            | -0,815                              | -0,795        | 17 | -0,251                     | -0,578        | 18 | 35                           |
| <b>AVERAGE</b> | <b>-0,761</b>                       | <b>-0,760</b> | /  | <b>-0,297</b>              | <b>-0,577</b> | /  | <b>49</b>                    |
| Le Mona        | -0,811                              | -0,801        | 9  | -0,161                     | -0,986        | 9  | 36                           |
| Lahage         | -0,882                              | -0,886        | 9  | -0,361                     | -0,882        | 9  | 39                           |
| Berat          | -0,819                              | -0,794        | 9  | -0,101                     | -0,752        | 9  | 45                           |
| <b>AVERAGE</b> | <b>-0,837</b>                       | <b>-0,827</b> | /  | <b>-0,208</b>              | <b>-0,873</b> | /  | <b>40</b>                    |

558

559

560

561 Table 3: Comparison between observed and retrieved  $w_g$ , from biangular and bipolarization  
562 CAROLS configurations (34H0H, 34V0V, 34VH), for the 14 soil moisture observation sites  
563 used in this study, using the 17 SMOSMANIA transect flights (Table 1). Correlation  
564 coefficients, root mean square error (RMSE, in units of  $m^3m^{-3}$ ) and  $F$ -Test  $p$ -values are  
565 presented. In the right column, two observation numbers are indicated for PRG and CDM  
566 stations: the number of valid observations for (left) 34H0H and 34V0V configurations and  
567 (right) 34VH. NS (non significant), \*, \*\*, \*\*\*, \*\*\*\* stand for  $p$ -values greater than 0.05,  
568 between 0.05 and 0.01, between 0.01 and 0.001, between 0.001 and 0.0001 and below 0.0001,  
569 respectively.

|            | 34H0H |       |            | 34V0V |       |            | 34VH |       |            | $n$  |
|------------|-------|-------|------------|-------|-------|------------|------|-------|------------|------|
|            | $r$   | RMSE  | $p$ -value | $r$   | RMSE  | $p$ -value | $r$  | RMSE  | $p$ -value |      |
| SBR        | 0.50  | 0.015 | NS         | 0.49  | 0.014 | NS         | 0.50 | 0.015 | NS         | 17   |
| URG        | 0.81  | 0.048 | ***        | 0.69  | 0.051 | **         | 0.86 | 0.044 | ***        | 17   |
| CRD        | 0.74  | 0.017 | **         | 0.72  | 0.018 | **         | 0.73 | 0.018 | **         | 17   |
| PRG        | 0.60  | /     | NS         | 0.59  | 0.025 | NS         | 0.84 | 0.021 | **         | 4/13 |
| CDM        | 0.49  | 0.021 | NS         | 0.42  | 0.019 | NS         | 0.77 | 0.022 | **         | 6/15 |
| LHS        | 0.63  | 0.033 | *          | 0.57  | 0.032 | NS         | 0.67 | 0.034 | *          | 17   |
| SVN        | 0.68  | 0.034 | *          | 0.62  | 0.033 | *          | 0.68 | 0.034 | *          | 17   |
| MNT        | 0.93  | 0.015 | ****       | 0.87  | 0.019 | ****       | 0.93 | 0.015 | ****       | 17   |
| SFL        | 0.75  | 0.027 | **         | 0.72  | 0.027 | **         | 0.71 | 0.027 | *          | 17   |
| MTM        | 0.58  | 0.014 | NS         | 0.57  | 0.014 | NS         | 0.53 | 0.013 | NS         | 17   |
| LZC        | /     | /     | /          | /     | /     | /          | /    | /     | /          | /    |
| NBN        | 0.77  | 0.021 | **         | 0.70  | 0.021 | **         | 0.85 | 0.019 | ***        | 17   |
| Le<br>Mona | 0.92  | 0.029 | **         | 0.83  | 0.038 | *          | 0.88 | 0.034 | *          | 9    |
| Lahage     | 0.92  | 0.022 | **         | 0.91  | 0.023 | **         | 0.90 | 0.024 | **         | 9    |
| Berat      | 0.77  | 0.025 | NS         | 0.71  | 0.025 | NS         | 0.70 | 0.025 | NS         | 9    |

570

571

572 Table 4:  $A_{wg}$ ,  $B_{wg}$  and  $C_{wg}$  regression coefficients from the multiple configuration regression  
 573 method applied to CAROLS data.

|            | $A_{wg}$ |        |       | $B_{wg}$ |        |        | $C_{wg}$ |       |       |
|------------|----------|--------|-------|----------|--------|--------|----------|-------|-------|
|            | 34H0H    | 34V0V  | 34VH  | 34H0H    | 34V0V  | 34VH   | 34H0H    | 34V0V | 34VH  |
| SBR        | 0.135    | 0.142  | 0.107 | -0.001   | -0.011 | 0.029  | 0.414    | 0.442 | 0.425 |
| URG        | 0.743    | 0.603  | 1.703 | -0.134   | -0.134 | -1.000 | 1.720    | 1.567 | 1.663 |
| CRD        | 0.127    | 0.110  | 0.155 | 0.024    | 0.020  | -0.010 | 0.447    | 0.446 | 0.425 |
| PRG        | 0.109    | 0.044  | 0.715 | 0.006    | 0.008  | -0.272 | 0.533    | 0.433 | 1.019 |
| CDM        | 0.089    | 0.034  | 0.636 | 0.015    | 0.018  | -0.257 | 0.595    | 0.512 | 0.957 |
| LHS        | 0.181    | 0.109  | 0.563 | 0.010    | 0.031  | -0.300 | 0.658    | 0.620 | 0.648 |
| SVN        | 0.338    | 0.265  | 0.640 | -0.085   | -0.083 | -0.332 | 0.674    | 0.660 | 0.637 |
| MNT        | 0.218    | 0.206  | 0.315 | 0.009    | 0.011  | -0.095 | 0.832    | 0.901 | 0.779 |
| SFL        | 0.150    | 0.141  | 0.161 | 0.033    | 0.032  | 0.018  | 0.620    | 0.660 | 0.617 |
| MTM        | 0.034    | 0.036  | 0.040 | 0.014    | 0.015  | 0.002  | 0.333    | 0.355 | 0.318 |
| LZC        | /        | /      | /     | /        | /      | /      | /        | /     | /     |
| NBN        | 0.123    | 0.091  | 0.468 | -0.009   | -0.007 | -0.291 | 0.443    | 0.433 | 0.396 |
| Le<br>Mona | 2.569    | -0.415 | 0.852 | -1.956   | 0.666  | -0.472 | 1.048    | 0.687 | 0.770 |
| Lahage     | -1.085   | -0.078 | 0.270 | 1.255    | 0.354  | 0.025  | 0.801    | 0.806 | 0.824 |
| Berat      | -1.726   | -0.025 | 0.087 | 1.719    | 0.199  | 0.086  | 0.460    | 0.530 | 0.542 |

574

575

576 Table 5 : Comparison between observed and retrieved  $w_g$ , from SMOS brightness  
 577 temperatures, using the  $A_{wg}$ ,  $B_{wg}$  and  $C_{wg}$  regression coefficients from the CAROLS 34VH  
 578 configuration.

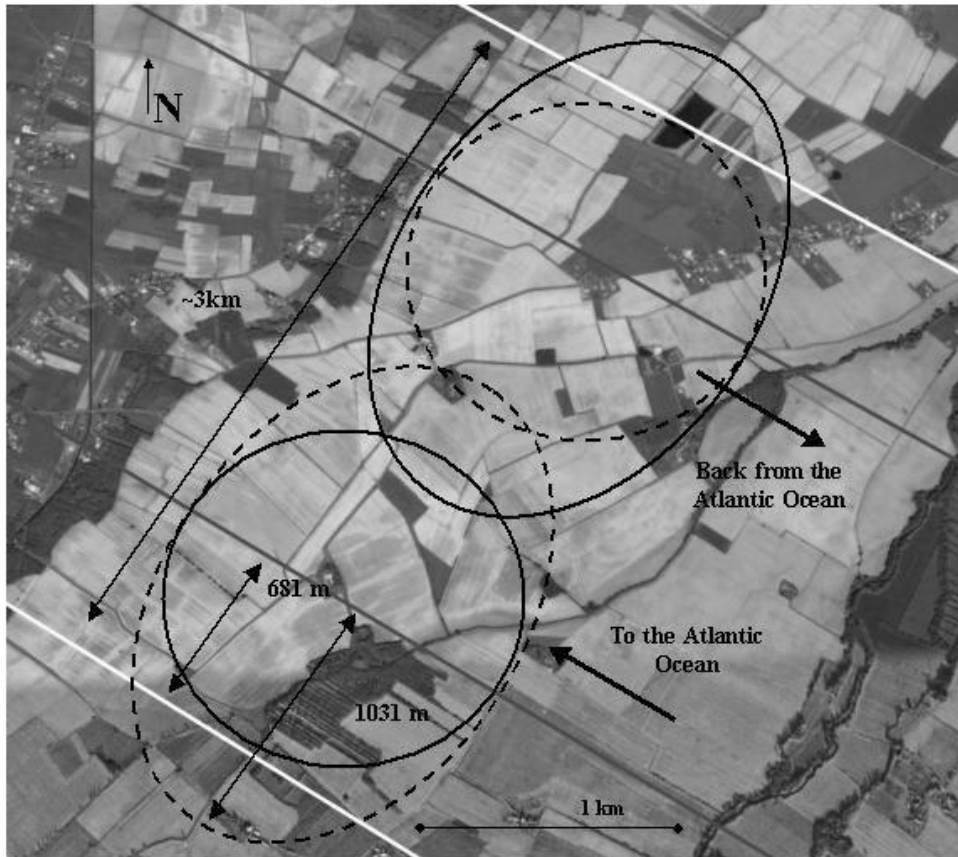
|     | 34VH |                          |            |     |
|-----|------|--------------------------|------------|-----|
|     | $r$  | RMSE<br>( $m^3 m^{-3}$ ) | $p$ -value | $n$ |
| SBR | 0.37 | 0.032                    | ***        | 96  |
| URG | 0.14 | 0.117                    | NS         | 44  |
| CRD | 0.25 | 0.043                    | *          | 90  |
| PRG | 0.4  | 0.059                    | **         | 61  |
| CDM | 0.32 | 0.057                    | **         | 75  |
| LHS | 0.14 | 0.073                    | NS         | 63  |
| SVN | 0.25 | 0.091                    | NS         | 57  |
| MNT | 0.43 | 0.089                    | ****       | 107 |
| SFL | 0.60 | 0.061                    | ****       | 97  |
| MTM | 0.30 | 0.037                    | *          | 68  |
| NBN | 0.29 | 0.044                    | *          | 55  |

579

580



582  
583 Figure 1: Map illustrating the SMOSMANIA network located in southwestern France (white  
584 crosses) forming a 400 km transect between the Atlantic ocean and the Mediterranean Sea.  
585 The stations are equipped with sensors measuring volumetric soil moisture content at various  
586 depth. The white line is for the CAROLS flights.

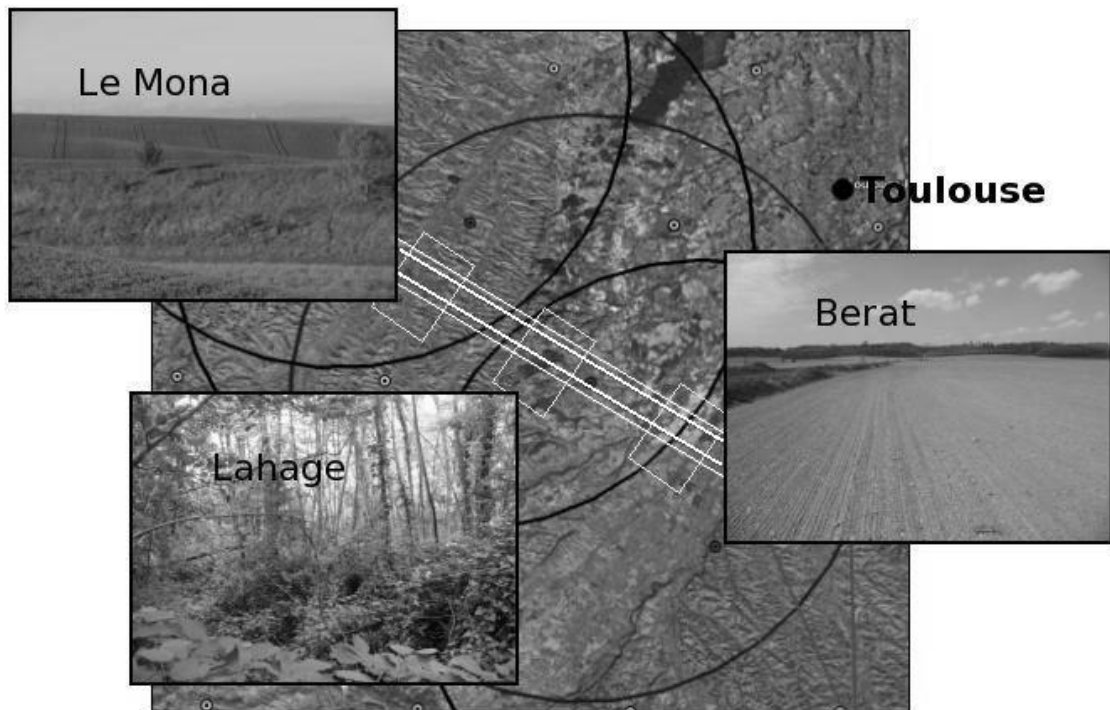


587

588 Figure 2: Schematic view of the surface at the Berat site, observed by the CAROLS

589 instrument during a flight, at 2000m asl.





590

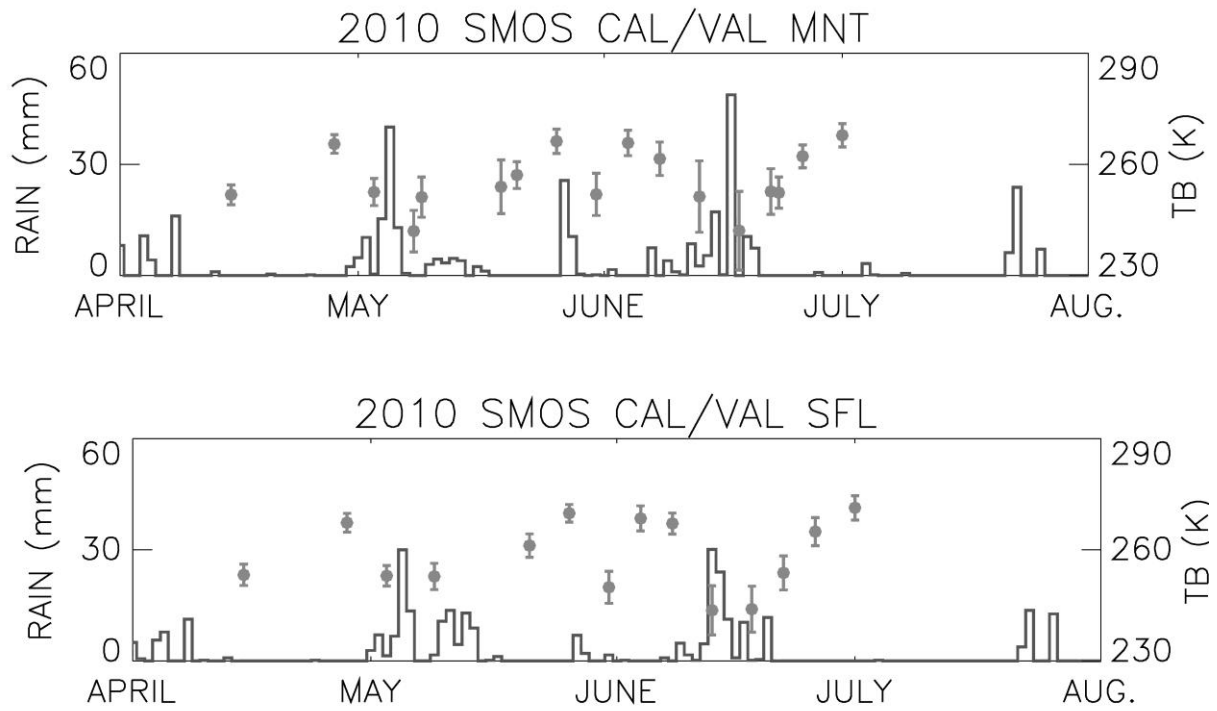
591 Figure 3: Three additional sites (white boxes) within a SMOS pixel (circles), at the southwest  
592 of Toulouse (black dot), investigated together with the twelve stations of the SMOSMANIA  
593 network. In situ soil moisture measurements at these three sites are performed with manual  
594 ThetaProbes. White lines are for the CAROLS flights.



595

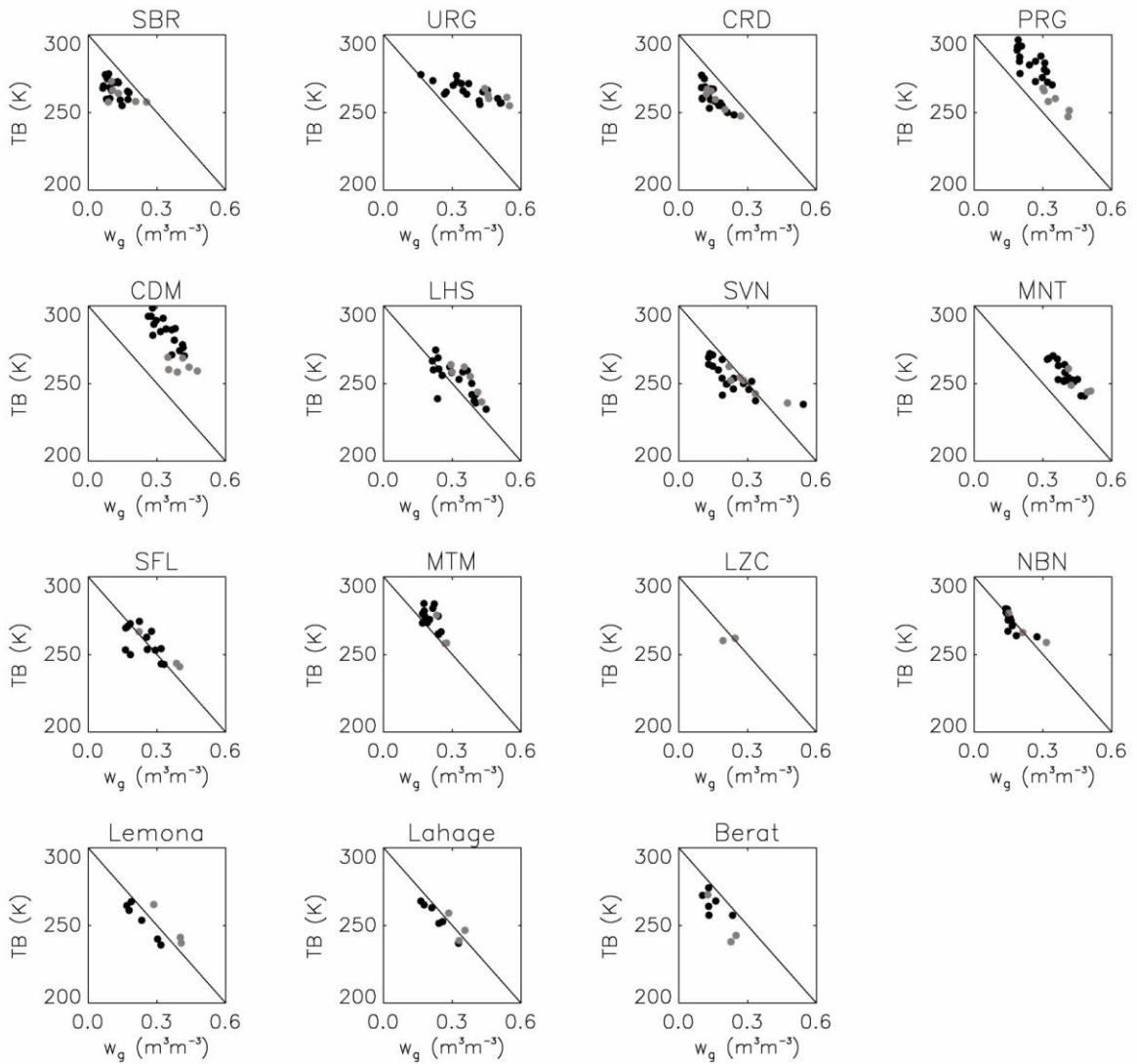
596 Figure 4 : Illustration of soil moisture acquisition on the Le Mona site for 2010 April 28. Soil

597 moisture is measured with ThetaProbes by two teams (yellow and red line).



598

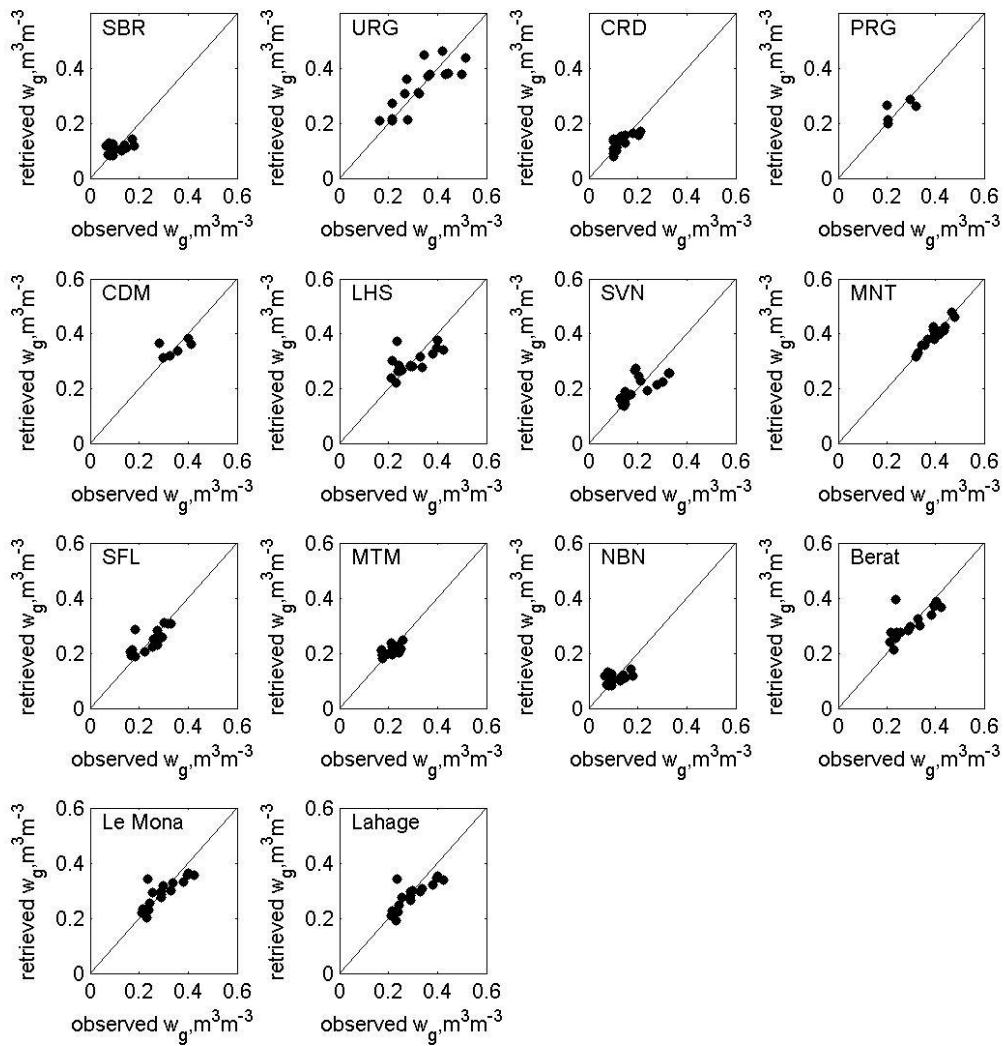
599 Figure 5: CAROLS's microwave  $T_b$  observations (dots) at nadir ( $0^\circ$ ) in vertical polarization  
 600 (V) with errors bars (standard deviation) for two stations of the SMOSMANIA network:  
 601 Montaut (MNT) and Saint-Felix de Lauragais (SFL). The observed rain is also presented  
 602 (line).



603

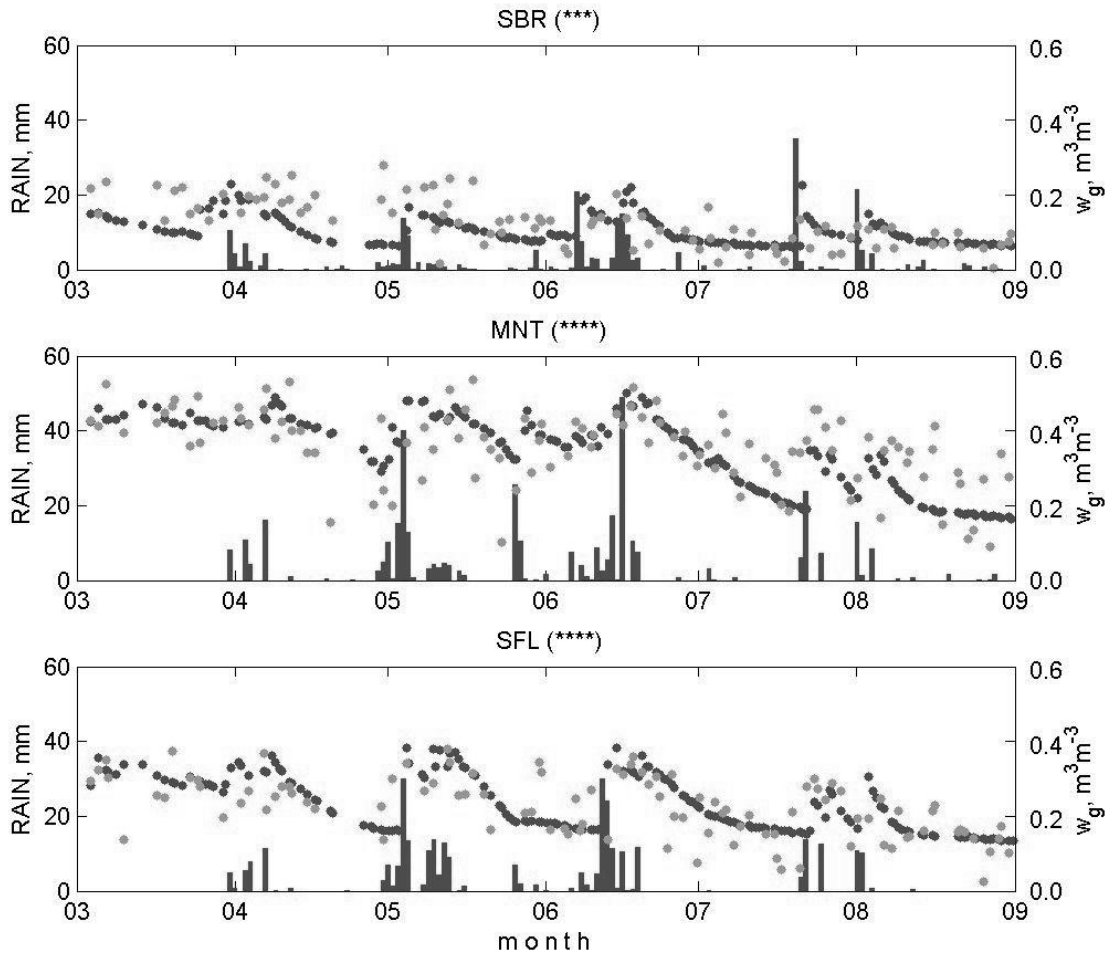
604 Figure 6 : CAROLS's microwave observations (nadir  $0^\circ$ , vertical V polarization) as a function  
 605 of the in situ soil moisture at 5cm, for 2009 (grey dots) and 2010 (black dots).

606



607  
 608 Figure 7: Retrieved versus observed  $w_g$  using the CAROLS brightness temperatures in the  
 609 34VH bipolarized regression, for the 14 soil moisture observations sites. There are no in situ  
 610 observations at the LZC station for the considered period.

611



612

613

614 Figure 8: Time series of surface soil moisture ( $w_g$ ) retrieved from SMOS  $T_b$  using CAROLS  
 615 empirical coefficients with the bipolarized approach (34HV), and observed in situ at three  
 616 SMOSMANIA stations, from March to September 2010. From top to bottom: Sabres (SBR),  
 617 Montaut (MNT), and Saint-Felix de Lauragais (SFL). Daily precipitation is represented by  
 618 vertical bars. Black dots are for the in situ  $w_g$ , and grey dots for SMOS-derived  $w_g$ . The level  
 619 of correlation significance between observed and retrieved  $w_g$  is given in brackets

Figure 1  
[Click here to download high resolution image](#)





Figure 2  
[Click here to download high resolution image](#)

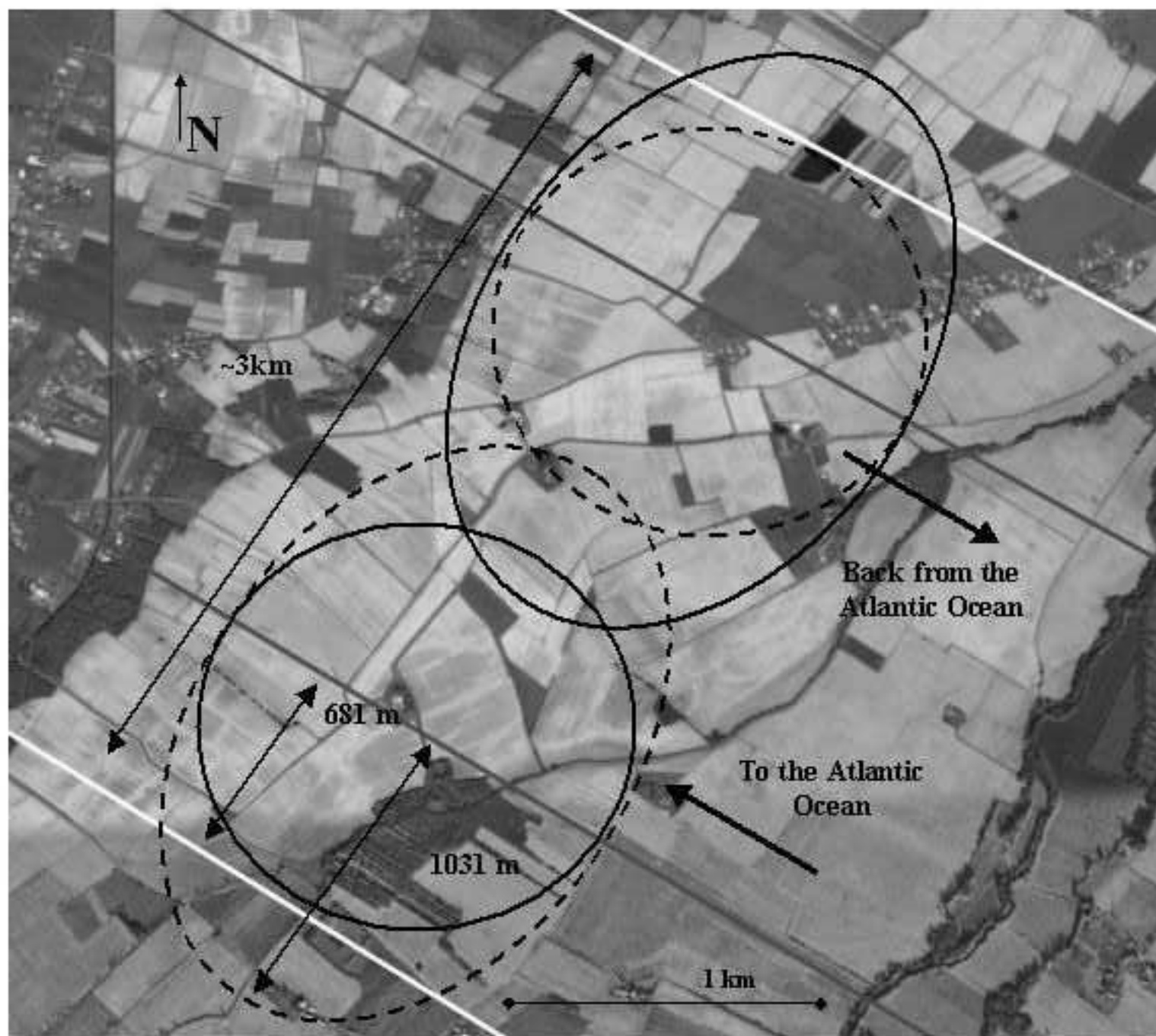




Figure 3  
[Click here to download high resolution image](#)

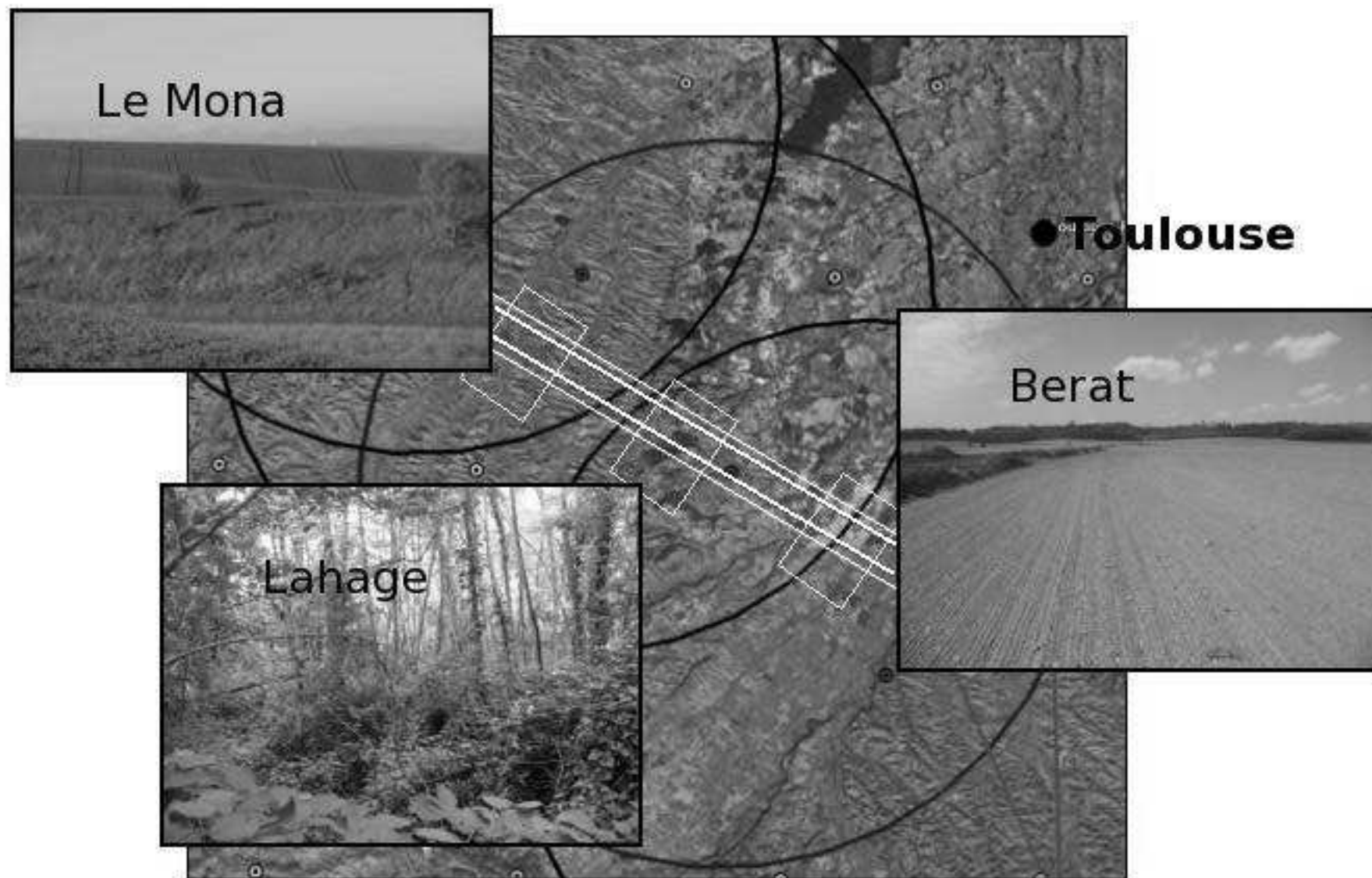


Figure 4  
[Click here to download high resolution image](#)



Figure 5  
[Click here to download high resolution image](#)

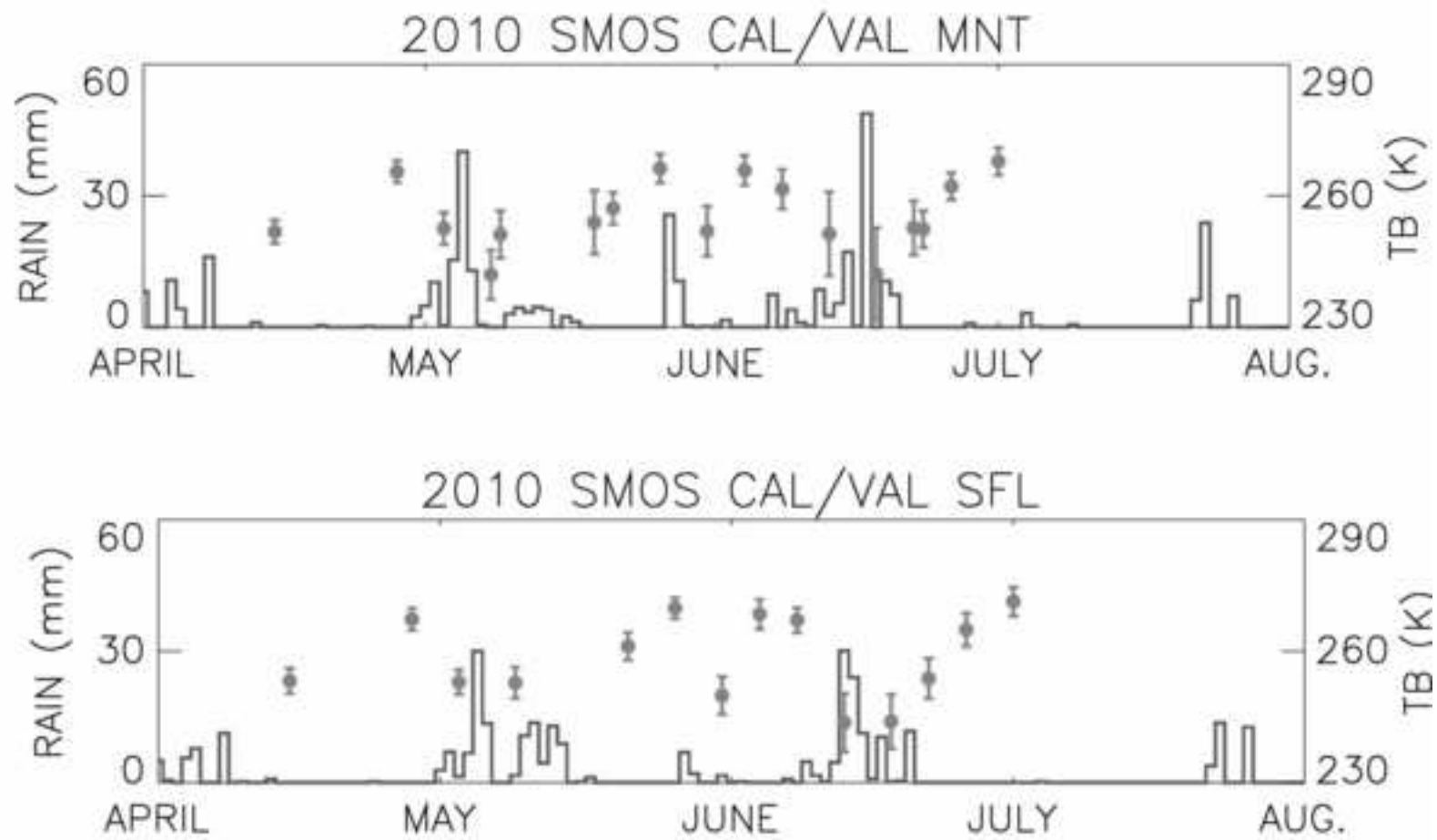


Figure 6  
[Click here to download high resolution image](#)

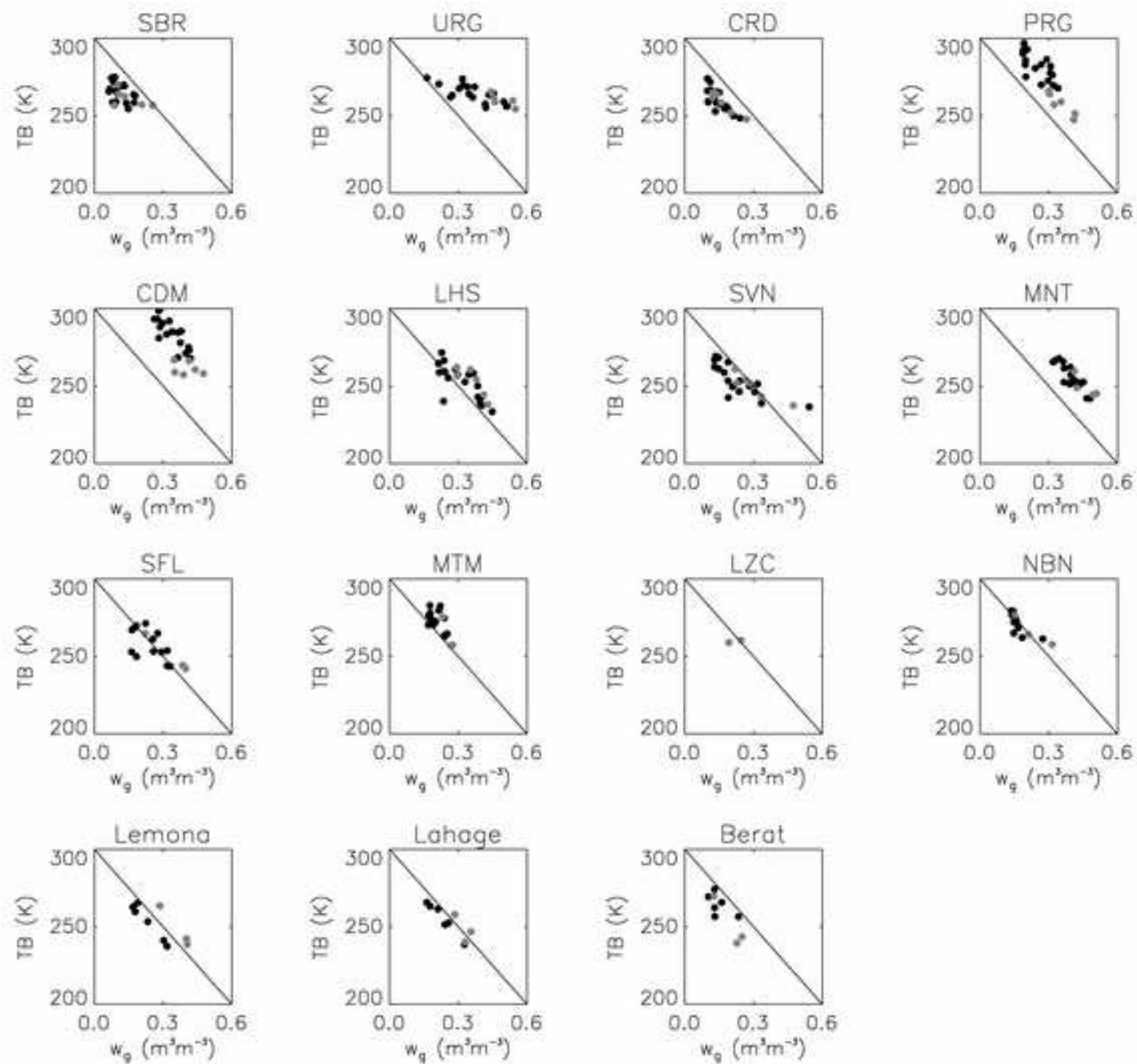




Figure 7  
[Click here to download high resolution image](#)

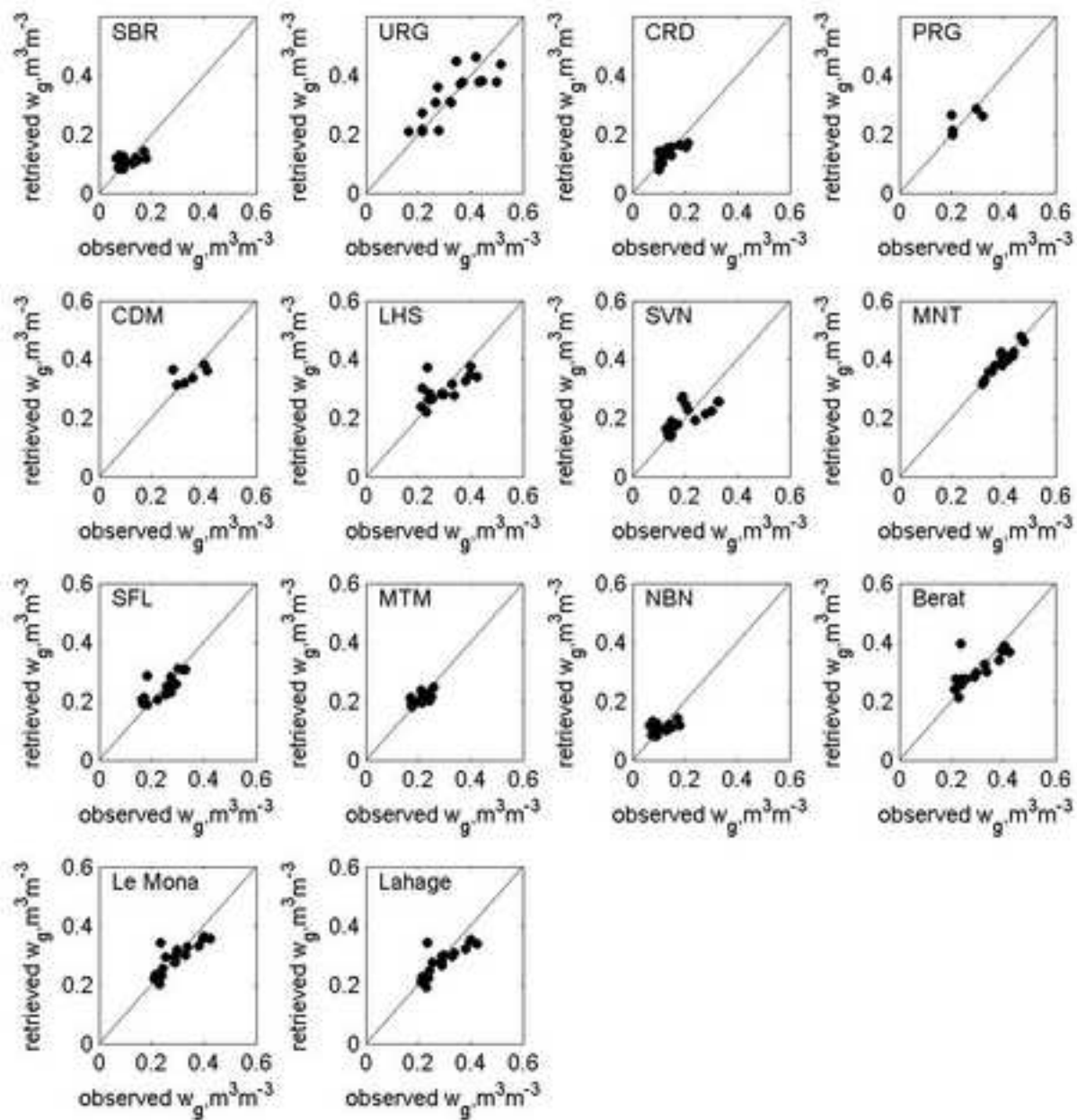


Figure 8  
[Click here to download high resolution image](#)

